Characterization of sulfate mineral deposits in central Thailand

Characterization of sulfate mineral deposits in central Thailand

Junichiro Kuroda[1,*], Hidetoshi Hara[2], Katsumi Ueno[3], Thasinee Charoentitirat[4], Teruyuki Maruoka[5], Takashi Miyazaki[1], Akira Miyahigashi[3] and Stefano Lugli[6]

[1] Atmosphere and Ocean Research Institute, the University of Tokyo, Kashiwa, Chiba 277-8564, Japan

[2] Geological Survey of Japan, National Institute of Advanced Industrial Science and Technology (AIST), Tsukuba, Ibaraki 305-8567, Japan

[3] Department of Earth System Science, Faculty of Science, Fukuoka University, Fukuoka 814-0180, Japan

[4] Department of Geology, Faculty of Science, Chulalongkorn University, Bangkok 10330, Thailand

[5] Graduate School of Life and Environmental Sciences, University of Tsukuba, ~~Tsukuba,~~ ~~Ibarak~~i 305-8572, Japan

[6] Dipartimento di Scienze Ghimiche e Geologiche, Universitá degli Studi di Modena e Reggio Emilia, Via Campi 103, 41125 Modena, Italy

*corresponding author: kuroda@aori.u-tokyo.ac.jp

Revised manuscript submitted to Island Arc, July 2016

Abstract

In this paper we present petrographic and geochemical data of sulfate mineral deposits in northeast Nakhon Sawan, central Thailand, and provide new constrains on their age. The deposits are made up mainly of strongly deformed nodular and massive gypsum in the upper part, and less deformed layered anhydrite in the lower part. They have been intruded by andesitic dikes that contain Middle Triassic zircons (~240 Ma). These dikes are probably part of the regional magmatic activity of the Sukhothai Arc during the Early to Middle Triassic. Sulfur ($\delta^{34}S$) and strontium ($^{87}Sr/^{86}Sr$) isotopic compositions of the sulfates range from 15.86‰ to 16.26‰ and from 0.70810 to 0.70817, respectively. Comparisons with the Phanerozoic seawater isotopic evolution curve indicate that those values are best explained by precipitation of the sulfates from Carboniferous seawater, in particular seawater of late Mississippian age (~326 Ma), and this would be consistent with previous studies of calcareous fossils in the limestones that crop out around this site. Our interpretation is that evaporitic gypsum was originally precipitated from hypersaline seawater on a shallow lagoon or shelf on the Khao Khwang Platform during the Serpukhovian, and that this gypsum changed to anhydrite during early burial. The anhydrite was then cut by andesitic dikes during the Middle Triassic, and more recently the upper part of which was rehydrated during exhumation to form secondary gypsum near the surface.

Key words: sulfate evaporites, strontium isotopes, sulfur isotopes, Carboniferous

INTRODUCTION

Calcium sulfate deposits (gypsum and anhydrite) of Paleozoic age are distributed around the Loei–Wang Saphung and Nakhon Sawan areas of mainland Thailand (e.g., Jacobson *et al*. 1969; Chonglakmani *et al*. 1983; El Tabakh & Utha–Aroon 1998; Ueno & Charoentitirat 2011). Among these, the sulfate deposits in the Loei–Wang Saphung area of northeast Thailand have been investigated in drilled cores (Utha–Aroon & Surinkum 1995; Surakotra *et al*. 2005; Surakotra 2011). Based on the occurrence of fusulinids from a limestone interval above the gypsum–anhydrite deposits, a late Moscovian (Pennsylvanian/late Carboniferous) age has been proposed for the sulfate deposits (Fontaine *et al*. 1997). However, the age of the gypsum–anhydrite itself still remains unknown, because the stratigraphic relationship between the sulfate deposits and the fossil-bearing limestone is unclear from borehole data (Surakotra *et al*. 2005). Large exposures of the sulfate deposits are found in quarries in northeastern Nakhon Sawan Province of central Thailand (Fig. 1), and some are still exploited by mining companies. In contrast to the Loei–Wang Saphung area, only a few studies have examined the deposits in the Nakhon Sawan area, and as yet there is no direct evidence for their age.

In this paper we characterize the sulfate mineral deposits based on petrographic observations, major and trace element compositions, and isotopic compositions of the sulfur ($\delta^{34}S$) and strontium ($^{87}Sr/^{86}Sr$) in order to assess their origin, the processes of precipitation, and the nature of diagenetic alteration. If the deposits were precipitated from seawater, their $\delta^{34}S$ and $^{87}Sr/^{86}Sr$ values could be used to constrain their age by making comparisons with the global reference curves of $\delta^{34}S$ (Kampschulte & Strauss 2004) and $^{87}Sr/^{86}Sr$ (McArthur *et al*. 2012) for Phanerozoic seawater. Sr isotopic record

is particularly useful because of well-homogenized isotopic composition through the global oceans due to its long residence time. Although $\delta^{34}S$ values are different for sulfate evaporites and carbonate-associated sulfur, they basically show parallel trends with offsets that are generally less than 4‰ through the Phanerozoic (Kampschulte & Strauss 2004). The seawater $^{87}Sr/^{86}Sr$ curve has been compiled for the Phanerozoic by McArthur *et al*. (2012) and is stored in a database called LOWESS.

The sulfate rock bodies are intruded by igneous dikes. We investigated petrography and geochemistry of the igneous dikes, and conducted U-Pb dating of zircons separated from the igneous intrusions to constrain the upper (younger) limit of the formation age of the sulfate rock body.

GEOLOGICAL SETTING

The basement rocks in Thailand can be divided into three geotectonic units; from west to east, the Sibumasu Block, the Sukhothai Zone, and the Indochina Block (Ueno & Charoentitirat 2011) (Fig. 2 A). The Sibumasu Block represents the peri-Gondwanan terrane, containing upper Carboniferous to lower Permian glaciogenic diamictites with Gondwanan fauna and flora, and middle–upper Permian platform carbonates. On its eastern side, a peculiar geotectonic domain called the Inthanon Zone can be defined; in this zone, Paleo-Tethyan oceanic rocks, made up of Carboniferous to Permian seamount carbonate rocks associated with greenstones and Middle Devonian to Middle Triassic radiolarian cherts, are widely exposed as tectonic outliers that rest on the underlying pre-Devonian basement (Cambrian sandstone and Ordovician limestone). The Sukhothai Zone is mainly made up of deformed Paleozoic to Mesozoic sedimentary and volcanic rocks. Triassic I-type granitoids are also present, and they suggest a

subduction-related tectonic setting and a volcanic arc that developed along the margin of the Indochina Block. To the east, upper Paleozoic shallow-marine carbonate rocks with diverse Tethyan faunas are widely distributed along the western margin of the Indochina Block. The Indochina Block, which occupies the eastern half of mainland Thailand, is part of the South China and Indochina Superterrane (Metcalfe 2000). It has been considered to be within the paleo-equatorial region since its Early Devonian rifting from Gondwana.

In the eastern part of the Nakhon Sawan area, the sedimentary rocks consist mainly of 1) Permian carbonate rocks of the Tak Fa Formation of the Saraburi Group, and 2) small amounts of Carboniferous strata (Fig. 2 B). These sedimentary rocks are widely distributed along the western margin of the Khorat Plateau of northeast Thailand, and this plateau is a part of the Indochina Block (El Tabakh & Utha–Aroon 1998; Ueno & Charoentitirat 2011; Ueno *et al*. 2012). The Carboniferous rocks have been found in several locations around Chon Daen, east of Nakhon Sawan (Chonglakmani *et al*. 1983; Fontaine *et al*. 1983; Ueno & Charoentitirat 2011), and they can be described as follows. A basal chert–volcanic tuff succession is overlain by dark-gray limestone that locally contains abundant foraminifera and corals of Visean age (Fontaine *et al*. 1991). In turn, the limestones are overlain by shales, siltstones, sandstones, and thin limestone beds and lenses. The shales and siltstones contain trilobites, brachiopods, and solitary corals, and the thin limestone beds yield Visean foraminifera. In this area several large sulfate deposits (approximately 10 km × 10 km areal extent) are exposed in active quarries (Fig. 1), and the deposits are crosscut by andesitic dikes. The distribution of sulfate mineral deposits is closely associated with reddish shales and sandy shales that appear to overlie the Visean strata (Chonglakmani *et al*. 1983). This implies that the timing of sulfate

precipitation was close to the Mississippian–Pennsylvanian boundary (Ueno & Charoentitirat 2011), although direct age constraints have not yet been obtained.

MATERIALS AND METHODS

Investigated sulfate rock samples were taken from three quarries in the Chon Daen area, east of Nakhon Sawan (Fig. 1). In the Chao Phraya Mueang Rae quarry in the central part of this are (Fig. 1 D), sample 13112601 was taken from below an igneous dike and sample 13112602 from the contact between the dike and the sulfate deposit; samples 13112603 and 13112603' were taken from above the dike (Fig. 3 A). In the K-Mining quarry in the northern part of this area (Fig. 1 C), sample 13112604 was part of a sulfate mineral deposit, and sample 13112605 was from an andesitic dike, collected for zircon U–Pb dating (Fig. 3 B). Each sample was cut and polished before making thin sections using the dry method proposed by Owada *et al.* (2013) for fragile samples. In the SCG Mine in the southern part of this area (Fig. 1 E), more than 20 cores have been drilled previously, and some of them are stored in this company. Sediment in a core GYP13 comprises mainly of reddish to light gray soil and clay as overburden (0-12.7 m depth), heavily deformed, white to gray gypsum (12.7-37.4 m depth), and layered gray anhydrite (37.4-60.0 m depth) (Fig. 4 A). All other cores show similar sedimentary sequence, although none of them has reached the bottom of the anhydrite. We took whole round core samples (10-20 cm long) from the GYP13 core (Fig. 4 B). In some other wells (GYP5 and GYP9), andesitic dikes cut both gypsum and anhydrite. After removing outer part of each sample block or core to avoid any contamination, all samples were pulverized using an agate mortar in preparation for bulk-rock analysis.

The distributions of major elements (Na, Mg, Al, Si, S, K, Ca, Fe, and Sr) in an area

of 20 mm × 30 mm in thin sections was determined by X-ray elemental mapping using a JEOL JXA-8500F field–emission electron probe microanalyzer (FE–EPMA) at Japan Agency for Marine-Earth Science and Technology (JAMSTEC). Measurements were performed with a 15 kV accelerating voltage, a 50 nA specimen current, and a focused beam of <1 μm diameter. Characteristic X-rays of all elements were measured from K-lines using a wavelength-dispersive spectrometer (WDS). Elemental compositional maps were obtained by scanning samples in stages, counting X-rays at each pixel, and with a 40 ms counting time. Details of the methods of sample preparation and the measurement conditions are given in Kuroda *et al*. (2005).

For bulk-rock major element, trace element, and Sr isotope analyses, samples were dissolved overnight with ~30% HCl at 120 °C. After heating to dryness, each sample was re-dissolved in 3% HNO_3. Subsamples were taken for inductively coupled plasma–mass spectrometry (ICP–MS) analysis, and diluted further with 3% HNO_3. Major and trace element concentrations were measured using a Thermo iCap quadrupole ICP–MS. Calibrations for each element have been given by Kuroda *et al*. (2007, 2016) and Hara *et al*. (2010). Analytical uncertainties (as relative standard deviation) for the bulk rock analysis were better than 3% for major elements, and better than 5% for trace elements.

Concentrations and stable isotopic compositions of sulfur were determined in powdered samples using an EA/IRMS (elemental analyzer/isotope–ratio mass spectrometer) system (Isoprime-EA, Isoprime) at the University of Tsukuba. The analytical procedures and conditions have been described by Maruoka *et al*. (2003). The sulfur isotopic compositions are expressed in terms of $\delta^{34}S$ (‰) relative to the Vienna Canyon Diablo Troilite (V-CDT) standard. The isotopic compositions of sulfur were determined with a precision of ± 0.2‰ (1σ). Two standard reference materials for sulfur

(IAEA-S-1 and 2) were used for calibrating sulfur contents and for correcting the instrumental mass discrimination of the IRMS.

Separation of Sr for isotopic analysis was carried out at JAMSTEC, using a method described by Roveri *et al*. (2014), with slight modifications. Sr was separated using Eichrom Sr Spec resin. Matrix elements were eluted in 6M HNO_3 and 3M HNO_3 before collecting Sr with 0.05M HNO_3. The total procedural blank for Sr samples prepared using this method was less than 10 pg. Samples were loaded onto single Re filaments with a Ta-activator (Takahashi *et al*. 2009), and the Sr isotopic composition of each sample was measured with a Thermo Scientific TRITON TI thermal ionizing mass spectrometer at JAMSTEC (Takahashi *et al*. 2009). The data were acquired in static multi-collection mode, and computed from 10 blocks of 15 cycles with an integration time of 15 sec for each cycle. The $^{87}Sr/^{86}Sr$ ratio was normalized for mass fractionation using an exponential law correction to the $^{86}Sr/^{88}Sr$ ratio of 0.1194. Analytical accuracy was evaluated by measuring NIST SRM 987, which provided readings of 0.7102455 ± 0.0000011 (2 S.D., $n = 3$) during the course of this study. The 2 standard error value of internal precision on an individual analysis was between 0.000008 and 0.000012. We did not correct for interference of ^{87}Rb because ^{87}Rb was not detected. The Sr isotope measurements were performed with an ^{88}Sr ion beam intensity of 3–5 V.

U–Pb dating was carried out for zircons in the andesitic dike sample 13112605 (Fig. 1 C). Zircons were separated using isodynamic magnetic and sodium polytungstate (SPT) heavy liquid separation techniques. Zircon grains were picked randomly from this concentrate, and mounted on and embedded in a Teflon sheet. Cathodoluminescence (CL) imaging was performed to observe the internal structures and zonation patterns of the zircons, and to select suitable sites for U–Pb dating using

SEM–EDS (JEOL JSM-6610 LV) equipped with a CL system (Gatan Mini CL) at the Geological Survey of Japan (GSJ). For the U–Pb age determinations, the U–Pb isotope abundance ratio was analyzed using laser ablation quadrupole–type ICP–MS (Agilent7700x, housed at Nagoya University), following the methods of Orihashi *et al*. (2008) and Kouchi *et al*. (2015). Analyses were performed with a spot size of 25 μm, a 10 Hz repetition rate, an energy density of 11.7 J cm^{-2}, and using a 213 nm solid state laser ablation system (ESi/New Wave Research NWR213). Calibration and data quality control were undertaken using standard zircons of 91500 and NIST SRM 610 at GSJ. All ages were calculated and concordia diagrams were made using Isoplot v.3.75 (Ludwig 2012).

RESULTS

PETROGRAPHIC CARACTERISTICS OF THE SULFATE DEPOSITS

The sulfate rocks consist mostly of heavily sheared gray to light gray massive microcrystalline gypsum (Fig. 3). In the drilled cores at the SCG Mine, the gypsum is underlain by layered gray anhydrite (Fig. 4 A). Unlike to the overlying gypsum, the anhydrite beds are much less deformed (Fig. 4 B). This implies that the top part of the anhydrite body has been rehydrated to gypsum due to exhumation, and that the heavily sheared structures in the gypsum samples were formed by recrystallization of anhydrite (i.e., volume increase due to rehydration). Same process has been reported from another sulfate rock body in Loei-Wang Saphung area (Surakotra, 2011).

In some cases a faint layering can be recognized in the gypsum and anhydrite, made evident by thin microcrystalline carbonate layers. Veneers of this carbonate outline vertically aligned centimetric gypsum nodules that resemble pseudomorphs of vertically

aligned selenite crystals. However, the nodules appear to have been strongly sheared during deformation and flow of the sulfate rock, and the original sedimentary features seem to have been completely obliterated.

Sample 13112601 consists mainly of microcrystalline gypsum with minor amounts of granular xenotopic gypsum and prismatic idiotopic gypsum. Very thin streaked-out fragments of silicate minerals have been deformed to form S-shape fold patterns (Fig. 5 A). Gypsum grains have been deformed by ductile flow, while laminae of silicate minerals have been partly disaggregated by brittle deformation into granules. The textures indicate that the gypsum originated by the hydration of former anhydrite (Lugli 2001).

Sample 13112602, which was taken from the contact zone between an andesitic dike and the sulfate deposit, is composed of xenotopic granular to idiotopic prismatic gypsum crystals up to 3 mm in size (Fig. 5 B). Deformed patches of microcrystalline gypsum a few mm in size are also present. Streaked-out fragments of silicate minerals are crosscut by veins of fibrous and prismatic gypsum crystals. As with sample 13112601, the gypsum crystals in 13112602 have been deformed by ductile flow, while the silicate layers have been boudinaged due to brittle deformation.

Sample 13112603 is laminated and consists of xenotopic granular to idiotopic prismatic gypsum crystals (Fig. 5 C) up to 3 mm in size. Some beds have vertically aligned crystals, especially the larger crystals. Other beds have a random orientation of crystals. Smaller crystals may be aligned to form thin, vertical or oblique linear structures up to 3 mm long. Again, this gypsum rock has textures that originated by the hydration of precursor anhydrite.

GEOCHEMICAL CARACTERISTICS OF THE SULFATE DEPOSITS

Concentrations of calcium (Table 1) and sulfur (Table 2) in gypsum samples range from 19.5 to 25.0 wt% and 16.3 to 17.1 wt%, respectively, which are typical of gypsum (~23 wt% Ca and ~19 wt% S). In contrast, the anhydrite samples have slightly higher Ca concentrations, ranging from 25.4 to 29.5 wt% (Table 1), which are close to the typical Ca value of anhydrite (~29 wt% Ca).

As comparison, we also measured the major and trace elements of gypsum from the Saline di Trapani, Sicily (JTG), where the gypsum has been artificially precipitated from present-day Mediterranean seawater (Table 1). The gypsum and anhydrite samples from Nakhon Sawan have lower concentrations of Mg and Sr than the gypsum from the Saline di Trapani, and these cations might have been leached out through dehydration from pristine gypsum to anhydrite during burial, and through rehydration of anhydrite to gypsum in a near-surface environment (e.g., the sulfate cycle of Murray 1964).

Primary anhydrite can only precipitate under relatively high temperatures and high salinity conditions as in supratidal sabkha evaporites (Warren 1999). However, our anhydrite samples show thin beddings (Fig. 4 B) suggesting a subaqueous origin rather than a supratidal evaporite. Therefore, the anhydrite beds seem to have formed secondary. The overlying gypsum is strongly deformed and recrystallized, and does not show original evaporite sedimentary structures such as selenite or twinned gypsum crystals, as commonly observed in pristine deposits (e.g., Lugli *et al*. 2010). Based on the lines of evidence we propose that the anhydrite was formed during burial at around 52 °C due to dehydration of the pristine evaporitic gypsum (e.g., Murray 1964; Shearman 1980; Testa & Lugli 2000). The lithological and mineralogical features of the Nakhon Sawan sulfate deposits resemble those of the Loei–Wang Saphung area, as

described by Surakotra *et al*. (2005), who suggested that the primary sulfate mineral was bedded selenite gypsum, precipitated on the floors of lagoons, lakes, or shallow shelves under arid climatic conditions. Likewise, we interpret that the sulfate deposits of Nakhon Sawan were originally precipitated in a shallow marine environment on the floor of a lagoon or shelf.

GEOCHEMICAL CARACTERISTICS OF THE IGNEOUS DIKES

The dikes are light to dark green in color, and 1–1.5 m in width, and they were intruded into the gypsum along vertical fractures that strike 20 °E at the sampling site of 13112605 in the northern quarry (Fig. 3 B). The SiO_2 and $Na_2 + K_2O$ contents of one of these dikes are 59.91 wt% and 2.03 wt%, respectively (Supporting Information Table S1), and the rock plots in the andesite field on the discrimination diagram of Wilson (1989). The andesitic dike is mainly made up of saussuritized plagioclase and small fractured phenocrysts of pyroxene (Fig. 5 D), and is locally cut by quartz and calcite veins. The groundmass contains glassy black seams, and is commonly altered to chlorite. The dike also contains xenoliths of dacitic, andesitic, and basaltic volcanic rocks, as well as abundant xenocrysts of quartz (Fig. 5 D).

At the sampling site of 13112602 in the southern quarry, an andesitic dike that intruded the gypsum deposit is composed mainly of plagioclase phenocrysts, is several to tens of centimeters in width, and has a horizontal attitude (Fig. 3 A). In sample 13112602, the dike exhibits laminae-like structures in the element maps of Mg, Si, and Fe (Fig. 6). The dike is characterized by cracks that are filled with gypsum, and this cracking might have occurred by volume expansion due to the rehydration of anhydrite to gypsum, with pore spaces filled with secondary gypsum.

SULFUR ISOTOPE RATIOS OF THE GYPSUM

The sulfur isotopic compositions ($\delta^{34}S$) of the gypsum fall in a narrow range between 15.86‰ and 16.26‰ (Table 2). Worden *et al*. (1997) demonstrated that the dehydration of gypsum into anhydrite does not involve significant isotopic fractionation or diagenetic redistribution of material. They showed that the stratigraphic variations of primary seawater $\delta^{34}S$ values in the Permian–Triassic were preserved in anhydrites in Abu Dhabi, despite post-depositional dehydration occurring at burial depths greater than ~1000 m. Although isotopic fractionation may have occurred on the submillimeter scale at Abu Dhabi, it was averaged out on the scale of individual centimeter-scale anhydrite nodules. We interpret that this was also the case for the gypsum samples at Nakhon Sawan. Sulfur isotopic compositions may also have been modified by the intrusion of the igneous dike. However, the $\delta^{34}S$ values of the sample nearest to the igneous dike (13112602) are identical to those located >20 m from the dikes (e.g., 13112604) (Table 2). This suggests that isotopic fractionation associated with the magmatic activity was negligible.

Because sulfur isotopic fractionation at the time of precipitation of sulfates from seawater is generally very small (e.g., Raab & Spiro 1991), we interpret the $\delta^{34}S$ values as primarily reflecting those of the co-existing seawater (brine), in other words, the $\delta^{34}S$ values of the gypsum can be correlated with the $\delta^{34}S$ values of contemporaneous ocean water sulfates (e.g., Paytan & Gray 2012).

STRONTIUM ISOTOPE RATIOS OF THE GYPSUM

Like sulfur isotopic compositions, the $^{87}Sr/^{86}Sr$ values of the gypsum and anhydrite

samples fall in a narrow range between 0.70811 and 0.70817 (Table 3). This strongly suggests that Sr isotopic composition is not influenced through the rehydration process from anhydrite to gypsum. In addition, it is also evident that andesitic intrusion did not alter the Sr isotopic composition of sulfate minerals significantly, because the $^{87}Sr/^{86}Sr$ value of the sample 13112603 which was taken nearby the intrusion also falls in the narrow range (0.70811). Sr isotopic compositions of evaporitic sulfates are known to be identical to those of ocean water, provided the brine (saline seawater) is fully connected with the ocean water. For example, the $^{87}Sr/^{86}Sr$ values of the primary lower gypsum that formed in the Mediterranean Sea during the first stage of the Messinian Salinity Crisis (5.97 to 5.61 Ma; Roveri *et al*. 2014) are almost identical to those of the coeval ocean water (~0.7090; McKenzie *et al*. 1988; McArthur *et al*. 2012), but show a slight decreasing trend (e.g., Müller & Mueller 1991; Flecker & Ellam 1999, 2006; Flecker *et al*. 2002; Roveri *et al*. 2014). This suggests that the dissolved Sr inventory in the Mediterranean was dominated by ocean water, but that there were minor but progressive contributions of Sr, fed into the sea from adjacent drainage basins. Much lower $^{87}Sr/^{86}Sr$ values have been observed for gypsum samples formed during the second and third stages of the salinity crisis (5.61 to 5.33 Ma; Roveri *et al*. 2014), when the connection of the Mediterranean with the global ocean was significantly restricted. In the second stage of the salinity crisis, thick halite was deposited in the deep basins, while the third stage is characterized by more significant influences of brackish water in the Mediterranean basins (e.g., CIESM 2007). Under the restricted basin conditions, Sr was mostly supplied from rivers, and the contribution of ocean water was diminished during these stages.

The sulfate mineral deposits in the Nakhon Sawan area are dominated by gypsum

and anhydrite, whereas halite, polyhalite, and kainite, which only precipitate from much denser saline water, are absent. Therefore, we interpret that the sulfate mineral deposits were precipitated from seawater that was still connected with ocean water, similarly to the primary lower gypsum deposits of the Mediterranean marginal basins during the first stage of the salinity crisis (Roveri *et al*. 2014). Therefore, the $^{87}Sr/^{86}Sr$ values of the Nakhon Sawan gypsum samples (Table 3) are inferred to reflect those of coeval ocean water.

AGES OF THE ANDESITE INTRUSION

Zircons from the andesitic dike sample 13112605 yield U–Pb ages that range from 231.7 ± 5.8 to 436.7 ± 11.8 Ma, with a single older Proterozoic age of 2404.7 ± 63.9 Ma (n = 33, Supporting Information Table S2). The results of U–Pb dating of zircons from the andesitic dike that are younger than 500 Ma are shown on a concordia diagram (Fig. S1 A) and on a relative age probability diagram (Fig. S1 B). The age distribution of zircons from the dike sample is characterized by multiple peaks, suggesting a variety of origins for the zircon grains (Fig. S1 B). The youngest age cluster is between 232 and 245 Ma (mean = 238.3 Ma), and the age cluster with the most intense peak ranges from 274 to 302 Ma (weighted mean age = 291.3 ± 4.8 Ma). Zircons from the dikes could have U–Pb ages that are older than the intrusion age if inherited and xenocrystic zircons were entrained into the dike magma (e.g., Keay *et al*. 1999; Shinjoe *et al*. 2003; Wang *et al*. 2012). The andesitic dike sample 13112605 contains xenoliths as well as xenocrysts of quartz. The quartz crystals seem to have originated from broken quartz veins and xenolithic materials of the host rocks. Assuming that the youngest cluster of zircon ages represents the timing of intrusion, the age of the andesitic dike is roughly 240 Ma, or

356 early Middle Triassic, and this corresponds to the timing of a major episode of
357 volcanism in the Sukhothai Arc (Barr *et al*. 2000; Srichan *et al*. 2009; Hara *et al*. 2013).
358 Trace element compositions of the igneous dike normalized to CI chondrite (Anders and
359 Grevesse, 1989) are best fit to that of the andesite rocks within the Sukhothai Arc
360 described by Srichan *et al*. (2009) (Fig. S2). These results indicate that the andesitic
361 dikes that intruded the gypsum deposits were part of the volcanic activity within the
362 Sukhothai Arc during the Early to Middle Triassic.
363
364 **DISCUSSION**
365 AGES OF THE SULFATE DEPOSITS
366 Both the $\delta^{34}S$ and $^{87}Sr/^{86}S$ values of our gypsum and anhydrite samples from the
367 Nakhon Sawan area are likely to reflect the values of the coeval ocean water from
368 which the sulfate evaporite was originally precipitated. This gives us a critical clue for
369 constraining the age of the sulfate evaporite, because we can compare our data with the
370 compiled database of the secular variation of isotopic compositions of strontium (e.g.,
371 McArthur *et al*. 2012) and sulfur (e.g., Kampschulte & Strauss 2004) (Fig. 7).
372 The $^{87}Sr/^{86}Sr$ values of our gypsum and anhydrite samples range from 0.70810 to
373 0.70817 (Table 3). During the last 500 Ma, this range of $^{87}Sr/^{86}Sr$ values in ocean water
374 has been observed in eight time windows, at ca. 26, 300, 326, 353–355, 364–367, 403–
375 406, 439, and 454 Ma (Fig. 7). Given the fact that both the gypsum and anhydrite
376 deposits are cut by a Middle Triassic andesitic dikes (~240 Ma), the youngest time
377 window of 26 Ma is excluded, and the likelihood is that the deposits are at least
378 Carboniferous or older.
379 The $\delta^{34}S$ values of our gypsum samples range between 15.86 and 16.26‰ (Table 2).

During the last 500 Ma, ocean water $\delta^{34}S$ values have changed in a range between +10‰ and +30‰ (Fig. 7) (Kampschulte & Strauss 2004; Paytan & Gray 2012). The recorded $\delta^{34}S$ values of evaporitic sulfates and carbonate-associated sulfates show relatively higher values (greater than +20‰) from the Cambrian through the Early Mississippian, and in the early Permian (Fig. 7). The $\delta^{34}S$ values of our gypsum samples fit well with the ocean water sulfate $\delta^{34}S$ curves between the Early Mississippian and Middle Pennsylvanian, and between the Late Permian and younger ages, but the latter possibility can be excluded by the presence of the cross-cutting Middle Triassic andesitic dikes and Sr isotope data.

There is a point on the ocean water curves that fits both the $^{87}Sr/^{86}Sr$ and $\delta^{34}S$ values of our gypsum and anhydrite samples, and that point (~326 Ma) is in the Serpukhovian (331-323 Ma) of the late Mississippian/the early Carboniferous (Fig. 7). The Tournaisian (359–347 Ma) of the Early Mississippian and the Gzhelian (304-229 Ma) of the Late Pennsylvanian are other possibilities. However, the ocean water sulfate $\delta^{34}S$ values for the Tournaisian are significantly higher than those of our gypsum samples, and although there are no available data for evaporitic sulfate $\delta^{34}S$ values in the Late Pennsylvanian, the Gzhelian $\delta^{34}S$ values for carbonate-associated sulfates are lower than our gypsum values (Fig. 7). Therefore, we suggest that the Tournaisian and the Gzhelian are less likely ages for our gypsum and anhydrite samples than the Serpukhovian.

ENVIRONMENTAL IMPLICATIONS

Previously, Ueno & Charoentitirat (2011) concluded the age of the sulfate mineral deposits in the Nakhon Sawan area fell on the Mississippian–Pennsylvanian boundary,

based on fossils in carbonate rocks in the vicinity. Our isotopic results are consistent with that age assessment, and we suggest that the sulfate evaporites were precipitated from seawater at the end of the Mississippian (Serpukhovian), in a shallow basin on a carbonate platform (Khao Khwang Platform) at the margin of the Indochina Block. The global seawater $^{87}Sr/^{86}Sr$ record shows a gradual increase through the Serpukhovian (Fig. 7). Our $^{87}Sr/^{86}Sr$ data from the core GYP13 does not show any change with depth (Table 3). This suggests that the sulfate rock body has precipitated within short duration, probably much shorter than the residence time of Sr in the ocean (4-5 million years at present).

Our results indicate that this site on the Khao Khwang Platform was subject to arid climatic conditions during the Serpukhovian. According to Metcalfe (2006), the Indochina Block was located between the paleoequator and 10 °N from the early Carboniferous to the early Permian. The emergence of arid climatic conditions in this equatorial region might be explained by the migration or meandering of the inter-tropical convergent zone (ITCZ) away from the equator during this time, or alternatively it could have been the result of a unique distribution of land and sea, and circulation of the atmosphere and ocean in this specific location, rather like present-day East Africa, where hyper-arid conditions prevail within an equatorial region (e.g., Le Houérou 2008).

On the western margin of the Indochina Block, similar sulfate deposits (gypsum–anhydrite) are also known in the Loei–Wang Saphung area of northeast Thailand (Surakotra *et al*. 2005). Those deposits have been assigned a late Moscovian (Middle Pennsylvanian) age, based on their stratigraphic relations with fossil-bearing limestones in borehole material (Fontaine *et al*. 1997; Surakotra *et al*. 2005), and this age is slightly

428 younger than that of the Nakhon Sawan sulfate deposits. In the Loei–Wang Saphung
429 area, mixed siliciclastic–carbonate deposition prevailed throughout most of
430 Pennsylvanian time, and normal open-marine conditions were common (Ueno &
431 Charoentitirat 2011). Moreover, it is well known that the Early Pennsylvanian
432 (Moscovian in particular) corresponds to a period of transgression in the record of
433 long-term sea-level change (e.g., Haq & Schutter 2008). These environmental settings
434 seem irreconcilable with the formation of a restricted hypersaline basin and the resultant
435 sulfate evaporitic deposits on the shelf of the Indochina Block. As inferred by Ueno &
436 Charoentitirat (2011), it seems more plausible to correlate the sulfate rock body in the
437 Loei–Wang Saphung area with that at Nakhon Sawan, given our present state of
438 knowledge. Further investigation is required to more precisely constrain the age of the
439 Loei–Wang Saphung deposits, using the same methods as those described in this paper.
440

441 **CONCLUSIONS**

442 The sulfate mineral deposits in the Nakhon Sawan area, central Thailand, are cut by
443 andesitic dikes, and U–Pb dating of zircons from the dike rocks indicates emplacement
444 in the Middle Triassic (~240 Ma). The dikes are probably related to regional magmatic
445 activity in the Sukhothai Arc during the Early to Middle Triassic. The sulfate deposits
446 are made up of thinly bedded anhydrite in the lower part, and heavily deformed massive
447 and nodular gypsum rocks in the upper part, which is rehydrated from the anhydrite.
448 The anhydrite was formed as a diagenetic product during burial through the dehydration
449 of the original pristine gypsum that had been precipitated from seawater in a shallow
450 lagoon or shelf environment. The sulfur and strontium isotopic compositions fit well
451 with the seawater values for Serpukhovian time (~326 Ma).

Based on various lines of evidence, we interpret the history of the sulfate mineral deposits as follows: 1) precipitation of pristine gypsum from seawater on the floor of a shallow lagoon or shelf on the Khao Khwang Platform during the Serpukhovian (Late Mississippian); 2) transformation of the pristine gypsum into anhydrite through dehydration at an early stage of burial; 3) emplacement of andesitic dikes into the sulfate deposits during the Middle Triassic; and 4) rehydration of the top part of anhydrite to form secondary gypsum near the surface following exhumation.

ACKNOWLEDGMENTS

We thank K. Yamamoto, K. Tsukada, and Y. Kouchi for their support with zircon U–Pb dating at Nagoya University; A. Owada, T. Sato, K. Fukuda, and E. Hirabayashi for their expertise in thin section preparation; Y. Kon for preliminary suggestions of U–Pb dating; M. Hamada for technical assistance with EPMA analysis at JAMSTEC; K. Ishikawa, B. S. Vaglarov, and K. Nagaishi for technical support in sample preparation and Sr isotopic analyses at JAMSTEC; T. Kurihara, R. Nohara, and M. Hirano for support with XRF analyses at Niigata University; and P. Charusiri, Y. Kamata, K. Hisada, N. Surakotra, N. Ohkouchi, and T. Yoshimura for constructive comments on an earlier draft of this manuscript. We also thank T. Tsujimori and an anonymous reviewer for critical and constructive comments on this manuscript. This research was supported financially by Grants-in-Aids from the Japan Society for the Promotion of Science (JSPS) to J. K. (No. 25400505), K. U., H. H., and J. K. (No. 25302010), and H. H. (No. 26302008).

REFERENCES

ANDERS E. & GREVESSE N. 1989. Abundance of the elements: Meteoritic and solar. *Geochimica et Cosmochimica Acta* **53**, 197–214.

BARR S.M., MACDONALD A.S., DUNNING G.R., OUNCHANUM P. & YAOWANOIYOTHIN W. 2000. Petrochemistry, U–Pb (zircon) age, and palaeotectonic setting of the Lampang volcanic belt, northern Thailand. *Journal of the Geological Society London* **157**, 553–63.

CHONGLAKMANI C., FONTAINE H. & VACHARD D. 1983. A Carboniferous–Lower Permian (?) section in Chon Daen area, Central Thailand. In: *Proceedings of the Conference on Geology and Mineral Resources of Thailand. Bangkok*, 18–19 November 1983, 1–5.

CIESM (Commission Internationale pour l'Exploration Scientifique de la mer Méditerranée) 2008. *The Messinian Salinity Crisis from mega-deposits to microbiology – A consensus report*. *CIESM Workshop Monographs* **33**, edited by F. Briand, 168 pp., CIESM, Monaco.

DEPARTMENT OF MINERAL RESOURCES (DMR), 1999. Geological Map of Thailand, Scale 1:1,000,000. Geological Survey Division, Department of Mineral Resources, Bangkok.

EL TABAKH M. & UTHA-AROON E. 1998. Evolution of a Permian carbonate platform to siliciclastic basin: Indochina Plate, Thailand. *Sedimentary Geology* **121**, 97–119.

FLECKER R. & ELLAM R.M. 1999. Distinguishing climatic and tectonic signals in the sedimentary successions of marginal basins using Sr isotopes: an example from the Messinian salinity crisis, Eastern Mediterranean. *Journal of the Geological Society (London)* **156**, 847–854.

499 FLECKER R. & ELLAM R.M. 2006. Identifying Late Miocene episodes of connection and
500 isolation in the Mediterranean–Paratethyan realm using Sr isotopes. *Sedimentary*
501 *Geology* **188–189**, 189–203.
502 FLECKER R., DE VILLIERS S. & ELLAM, R.M. 2002. Modelling the effect of evaporation
503 on the salinity–87Sr/86Sr relationship in modern and ancient marginal-marine
504 systems: the Mediterranean Messinian Salinity Crisis. *Earth and Planetary Science*
505 *Letters* **203**, 221–233.
506 FONTAINE H., LOVACHALASUPAPORN S., TIEN N.D. & VACHARD D. 1983. New data on
507 the Lower Carboniferous in Thailand. *CCOP Newsletter* **10** (1/2), 13–18.
508 FONTAINE H., SUTTETHORN V. & JONGKANJANASOONTORN Y. 1991. Carboniferous corals
509 of Thailand. *CCOP Technical Bulletin* **22**, 1–82.
510 FONTAINE H., SALYAPONGSE S., UTHA-AROON C. & VACHARD D. 1997. Age of
511 limestones associated with gypsum deposits in northeast and central Thailand: A first
512 report. *CCOP Newsletter* **21** (4), 6–10.
513 HAQ B.U. & SCHUTTER S.R. 2008. A chronology of Paleozoic sea-level change. *Science*
514 **322**, 64–8.
515 HARA H., KURIHARA T., KURODA J., ADACHI Y., KURITA H., WAKITA K., HISADA K.,
516 CHARUSIRI P., CHAROENTITIRAT T. & CHAODUMRONG P. 2010. Geological and
517 geochemical aspects of a Devonian siliceous succession in northern Thailand:
518 Implications for the opening of the Paleo-Tethys. *Palaeogeography,*
519 *Palaeoclimatology, Palaeoecology* **297**, 452–64.
520 HARA H., KON Y., USUKI T., LAN C.-Y., KAMATA Y., HISADA K., UENO K.,
521 CHAROENTITIRAT T. & CHARUSIRI P. 2013. U-Pb ages of detrital zircons within the
522 Inthanon Zone of the Paleo-tethyan subduction zone, northern Thailand: New

523 constraints on accretionary age and arc activity. *Journal of Asian Earth Sciences* **74**,
524 50–61.
525 JACOBSON H.S., PIERSON C.T., DANUASAWAD T., JAPAKASETR T., INTHUPUTI B.,
526 SIRIRATANAMONGKOL C., PRAPASSORNKUL S. & PHOLPHAN N. 1969. Mineral
527 investigations in northeastern Thailand. *U.S. Geological Survey Professional Paper*
528 **618**, 1–96.
529 KAMPSCHULTE A. & STRAUSS H. 2004. The sulfur isotopic evolution of Phanerozoic
530 seawater based on the analysis of structurally substituted sulfate in carbonates.
531 *Chemical Geology* **204**, 255–86.
532 KEAY S., STEELE D. & COMSTON W. 1999. Identifying granite sources by SHRIMP U-Pb
533 zircon geochronology: an application to the Lachlan foldbelt. *Contributions to*
534 *Mineralogy and Petrology* **137**, 323–41.
535 KOUCHI Y., ORIHASHI Y., OBARA H., FUJIMOTO T., HARUTA Y. & YAMAMOTO K. 2015.
536 Zircon U–Pb dating by 213 nm Nd: YAG laser ablation inductively coupled plasma
537 mass spectrometry: Optimization of the analytical condition to use NIST SRM 610
538 for Pb/U fractionation correction. *Chikyukagaku* (*Geochemistry*) **49**, 1–17 (in
539 Japanese with English abstract).
540 KURODA J., OHKOUCHI N., ISHII T., TOKUYAMA H. & TAIRA A. 2005. Lamina-scale
541 analysis of sedimentary components in Cretaceous black shales by chemical
542 compositional mapping: Implications for paleoenvironmental changes during the
543 Oceanic Anoxic Events. *Geochimica et Cosmochimica Acta* **69**, 1479–94.
544 KURODA J., OGAWA N.O., TANIMIZU M., COFFIN M.F., TOKUYAMA H., KITAZATO H. &
545 OHKOUCHI N. 2007. Contemporaneous massive subaerial volcanism and late
546 cretaceous Oceanic Anoxic Event 2. *Earth and Planetary Science Letters* **256**, 211–

23.

KURODA J., JIMÉNEZ-ESPEJO F.J., NOZAKI T., GENNARI R., LUGLI S., MANZI V., ROVERI M., FLECKER R., SIERRO F.J., YOSHIMURA T., SUZUKI K. & OHKOUCHI N. 2016. Miocene to Pleistocene osmium isotopic records of the Mediterranean sediments, *Paleoceanography* **31**, 148–166.

LE HOUÉROU H.N. 2009. *Bioclimatology and Biogeography of Africa*. Springer-Verlag, Berlin.

LUDWIG K.R. 2012. User's Manual for Isoplot 3.75. Special Publication. no. 5, Berkeley Geochronology Center, Berkeley, CA.

LUGLI S. 2001. Timing of post-depositional events in the Burano Formation of the Secchia valley (Upper Triassic, Northern Apennines), clues from gypsum–anhydrite transitions and carbonate metasomatism. *Sedimentary Geology* **140**, 107–22.

LUGLI S., MANZI V., ROVERI M. & SCHREIBER B.C. 2010. The Primary Lower Gypsum in the Mediterranean: A new facies interpretation for the first stage of the Messinian salinity crisis. *Palaeogeography, Palaeoclimatology, Palaeoecology* **297**, 83–99.

MARUOKA T., KOEBERL C., HANCOX P.J. & REIMOLD W.U. 2003. Sulfur geochemistry across a terrestrial Permian-Triassic boundary section in the Karoo Basin, South Africa. *Earth and Planetary Science Letters* **206**, 101–17.

MCARTHUR J.M., HOWARTH R.J. & SHIELDS G.A. 2012. Strontium isotope stratigraphy. *In* Gradstain F.M., Ogg J.G., Schmitz M.D. and Ogg G.M. (eds.) *The Geologic Timescale 2012*, Vol. 1, pp. 127–44, Elsevier.

MCKENZIE J.A., HODELL D.A., MUELLER P.A. & MUELLER D.W. 1988. Application of strontium isotopes to late Miocene-early Pliocene stratigraphy. *Geology* **16**, 1022–1025.

MCLENNAN S.M. 1989. Rare earth elements in sedimentary rocks: Influence of provenance and sedimentary processes. *In* Lipinand B. R. and Mckay G. A. (eds.) *Geochemistry and Mineralogy of Rare Earth Elements*. Reviews in Mineralogy 21, pp. 169–200, Mineralogical Society of America, Chantilly.

METCALFE I. 2000. The Bentong-Raub Suture Zone. *Journal of Asian Earth Sciences* **18**, 691–712.

METCALFE I. 2006. Palaeozoic and Mesozoic tectonic evolution and palaeogeography of East Asian crustal fragments: the Korean Peninsula in context. *Gondwana Research* **9**, 24–46.

MÜLLER D.W. & MUELLER P.A. 1991. Origin and age of the Mediterranean Messinian evaporites: implications from Sr isotopes. *Earth and Planetary Science Letters* **107**, 1–12.

MURRAY R.C. 1964. Origin and diagenesis of gypsum and anhydrite. *Journal of Sedimentary Petrology* **34**, 512–23.

ORIHASHI Y., NAKAI S. & HIRATA T. 2008. U–Pb age determination for Seven Standard Zircons using Inductively Coupled Plasma–Mass Spectrometry Coupled with Frequency Quintupled Nd-YAG (λ = 213 nm) Laser Ablation System: Comparison with LA-ICP-MS Zircon Analyses with a NIST Glass Reference Material. *Resource Geology* **58**, 101–23.

OWADA A., SATO T. & HIRABAYASHI E. 2013. New method for making petrographic sections of fragile rocks without using liquids as coolants or lubricants –dry method–. *Bulletin of Geological Survey of Japan* **64**, 221−224.

PAYTAN A. & GRAY E.T. 2012. Sulfur isotope stratigraphy. *In* Gradstain F.M., Ogg J.G., Schmitz M.D. and Ogg G.M. (eds.) *The Geologic Timescale 2012*, Vol. 1, pp. 167–80,

595 Elsevier.
596 RAAB M. & SPIRO B. 1991, Sulfur isotope variations during seawater evaporation with
597 fractional crystallization. *Chemical Geology* **86**, 323–333.
598 ROVERI M., LUGLI S., MANZI V., GENNARIA R. & SCHREIBER B.C. 2014. High-resolution
599 strontium isotope stratigraphy of the Messinian deep Mediterranean basins:
600 Implications for marginal to central basins correlation. *Marine Geology* **349**, 113–25.
601 SHEARMAN D.J. 1978. Evaporites of coastal sabkhas. *In* Dean W.E. and Schreiber B.C.
602 (eds.) *Marine Evaporites*. SEPM Short Course Note 4, pp. 6–42, SEPM Publication.
603 SHINJOE H., WADA Y., ORIHASHI Y., SUMII T. & NAKAI S. 2003. Possible presence of the
604 concealed Miocene granitic body to the south of Median Tectonic Line, Yoshino
605 district, Nara Prefecture, inferred from zircon U–Pb age of the granitic enclave in
606 dike. *Journal of the Geological Society of Japan* **109**, 689–96 (in Japanese with
607 English abstract).
608 SRICHAN W., CRAWFORD A.J. & BERRY R.F. 2009. Geochemistry and geochronology of
609 Late Triassic volcanic rocks in the Chiang Khong region, northern Thailand. *Island*
610 *Arc* **18**, 32–51.
611 SURAKOTRA N. 2011. Diagenesis of Laminated Loei-Wang Saphung Gypsum-Anhydrite
612 Deposits in the Northeastern Thailand. *In* Satarugsa P., Lertsirivorakul R., Kromkhun
613 K. and Promkotra S. (eds.) *Proceedings of the International Conference on Geology,*
614 *Geotechnology and Mineral Resources of INDOCHINA* (GEOINDO 2011), pp. 106–
615 15, Department of Geotechnology, Khon Kaen University, Khon Kaen.
616 SURAKOTRA N., PISUTHA-ARNOND V. & WARREN J.K. 2005. Some Characteristics of
617 Gypsum-Anhydrite Deposit in the Loei-Wang Saphung, Northeastern Thailand. *In*
618 Wannakao L., Youngme W., Srisuk K. and Lertsirivorakul R. (eds.) *Proceedings of*

the International Conference on Geology, Geotechnology and Mineral Resources of INDOCHINA (GEOINDO 2005), pp. 421–30, Department of Geotechnology, Khon Kaen University, Khon Kaen.

TAKAHASHI T., HIRAHARA Y., MIYAZAKI T., VAGLAROV B.S., CHANG Q., KIMURA J.-I. & TATSUMI Y. 2009. Precise determination of Sr isotope ratios in igneous rock samples and application to micro-analysis of plagioclase phenocrysts. *JAMSTEC Report of Research and Development* **2009**, 59–64.

TAYLOR S.R. & MCLENNAN S.M. 1985. The Continental Crust: Its Composition and Evolution. Blackwell Scientific Publications, Oxford.

TESTA G. & LUGLI S. 2000. Gypsum–anhydrite transformations in Messinian evaporites of central Tuscany (Italy). *Sedimentary Geology* **130**, 249–268.

UENO K. & CHAROENTITIRAT T. 2011. Carboniferous and Permian. *In* Ridd M.F., Barber A.J. and Crow M.J. (eds.) *The Geology of Thailand*, pp. 71–136, Geological Society of London.

UENO K., MIYAHIGASHI A., KAMATA Y., KATO M., CHAROENTITIRAT T. & LIMRUK S. 2012. Geotectonic implications of Permian and Triassic carbonate successions in the Central Plain of Thailand. *Journal of Asian Earth Sciences* **61**, 33–50.

UTHA-AROON C. & SURINKUM A. 1995. Gypsum exploration in Wang Saphung, Loei. *In* Youngme, W., Buaphan, C., Srisuk, K. & Lertsirivorakul, R. (eds.) *Proceedings of the International Conference on Geology, Geotechnology and Mineral Resources of INDOCHINA* (GEOINDO 1995), pp. 255–66, Department of Geotechnology, Khon Kaen University, Khon Kaen.

WANG Q. CHUNG S.-L., LI X.-H., Wyman D., Li Z.-X., Sun W.-D., Qiu H.-N., Liu Y.-S. & Zhu Y.-T. 2012. Crustal Melting and Flow beneath Northern Tibet: Evidence from

643 Mid-Miocene to Quaternary Strongly Peraluminous Rhyolites in the Southern
644 Kunlun Range. *Journal of Petrology* **53**, 2523–66.
645 WARREN J.K., 1999. Evaporites: their evolution and economics. Blackwell Scientific,
646 Oxford, UK. 438 p.
647 WILSON M. 1989. Igneous Petrogenesis: A Global Tectonic Approach. Springer,
648 Netherlands.
649 WORDEN R.H., SMALLEY P.C. & FALLICK A. E. 1997. Sulfur cycle in buried evaporites.
650 *Geology* **25**, 643–46.
651

652 **TABLES**

653 **Table 1**. Major and trace element concentrations of the gypsum and anhydrite samples measured by ICP–MS.

Sample name	Location	Lithology	Mg (μg g^{-1})	Al (μg g^{-1})	K (μg g^{-1})	Ca (wt.%)	Sc (μg g^{-1})	Ti (μg g^{-1})	V (μg g^{-1})	Cr (μg g^{-1})	Mn (μg g^{-1})	Fe (μg g^{-1})	Co (μg g^{-1})	Ni (μg g^{-1})	Cu (μg g^{-1})	Zn (μg g^{-1})	Sr (μg g^{-1})	Y (μg g^{-1})	Ba (μg g^{-1})	Pb (μg g^{-1})	U (μg g^{-1})
JTG†	Saline di Trapani, Sicily	Gypsum	625	158	291	22.6	0.485	682	0.377	0.762	7.16	76.1	1.11	4.48	0.399	0.386	1511	0.0815	1.30	2.51	0.0264
13112601	Chao Phraya Mueang Rae	Gypsum	141	183	75.0	22.3	0.522	678	0.764	0.654	11.5	134	5.85	5.14	1.82	1.49	745	0.140	1.44	0.131	0.300
13112602	Chao Phraya Mueang Rae	Gypsum	36.3	52.6	54.3	21.9	0.385	664	0.549	0.173	2.55	68.0	1.04	4.40	0.143	*n.d.*	785	0.174	1.26	0.0267	0.0320
13112603	Chao Phraya Mueang Rae	Gypsum	27.3	174	40.8	25.0	0.331	673	0.264	0.159	0.953	66.1	0.861	4.98	0.172	0.118	491	0.0411	0.694	0.0736	0.00922
13112603'	Chao Phraya Mueang Rae	Gypsum	36.2	44.1	30.6	21.6	0.311	644	0.476	0.256	3.44	57.9	0.611	3.92	0.065	*n.d.*	560	0.0780	0.911	0.0222	0.0893
13112604	K-Mining	Gypsum	29.0	106	19.3	19.5	0.232	529	0.276	0.082	1.22	53.0	0.374	3.54	*n.d.*	*n.d.*	810	0.0498	0.913	0.0193	0.0383
GYP13 12-13	SCG Mine (core)	Gypsum	*n.d.*	251	70.9	22.5	*n.a.*	*n.a.*	*n.a.*	*n.a.*	2.20	444	*n.a.*	*n.a.*	*n.a.*	*n.a.*	247	*n.a.*	2.173	*n.a.*	*n.a.*
GYP13 15-16	SCG Mine (core)	Gypsum	1932	20.0	210	22.4	*n.a.*	*n.a.*	*n.a.*	*n.a.*	5.30	353	*n.a.*	*n.a.*	*n.a.*	*n.a.*	538	*n.a.*	0.572	*n.a.*	*n.a.*
GYP13 22-23	SCG Mine (core)	Gypsum	*n.d.*	*n.d.*	156	23.3	*n.a.*	*n.a.*	*n.a.*	*n.a.*	*n.d.*	331	*n.a.*	*n.a.*	*n.a.*	*n.a.*	696	*n.a.*	0.418	*n.a.*	*n.a.*
GYP13 31-32	SCG Mine (core)	Gypsum	38.5	*n.d.*	233	24.0	*n.a.*	*n.a.*	*n.a.*	*n.a.*	*n.d.*	359	*n.a.*	*n.a.*	*n.a.*	*n.a.*	606	*n.a.*	0.158	*n.a.*	*n.a.*
GYP13 37-38	SCG Mine (core)	Anhydrite	*n.d.*	*n.d.*	286	25.4	*n.a.*	*n.a.*	*n.a.*	*n.a.*	2.32	347	*n.a.*	*n.a.*	*n.a.*	*n.a.*	742	*n.a.*	0.673	*n.a.*	*n.a.*
GYP13 43-44	SCG Mine (core)	Anhydrite	*n.d.*	*n.d.*	150	25.7	*n.a.*	*n.a.*	*n.a.*	*n.a.*	11.6	361	*n.a.*	*n.a.*	*n.a.*	*n.a.*	794	*n.a.*	0.138	*n.a.*	*n.a.*
GYP13 49-50	SCG Mine (core)	Anhydrite	87.7	*n.d.*	196	28.0	*n.a.*	*n.a.*	*n.a.*	*n.a.*	6.15	407	*n.a.*	*n.a.*	*n.a.*	*n.a.*	1000	*n.a.*	0.143	*n.a.*	*n.a.*
GYP13 57-58	SCG Mine (core)	Anhydrite	6.64	*n.d.*	182	29.5	*n.a.*	*n.a.*	*n.a.*	*n.a.*	0.806	418	*n.a.*	*n.a.*	*n.a.*	*n.a.*	1063	*n.a.*	0.355	*n.a.*	*n.a.*

654

655 † JAMSTEC in-house standard of gypsum rock reference material taken from the Saline di Trapani, Sicily.

656 *n.d.*: not detected, *n.a.*: not analyzed. Analytical uncertainties (as relative standard deviation) for the bulk rock analysis were better than

657 3% for major elements, and better than 5% for trace elements.

658

659 **Table 2**. Sulfur concentrations and stable sulfur isotopic compositions of the gypsum
660 samples from the quarries in the Chon Daen area, east of Nakhon Sawan.

Sample name	Location	Lithology	Total S (wt.%)	S.D.	$\delta^{34}S$ (‰ V-CDT)	S.D.
13112601	Chao Phraya Mueang Rae	Gypsum	16.3	1.3	15.855	0.199
13112602	Chao Phraya Mueang Rae	Gypsum	16.5	1.5	16.171	0.100
13112603	Chao Phraya Mueang Rae	Gypsum	17.1	1.4	16.151	0.091
13112604	K-Mining	Gypsum	16.6	2.3	16.258	0.123

661

662

663 **Table 3**. Sr isotopic ratios of the gypsum and anhydrite samples from the quarries in the
664 Chon Daen area, east of Nakhon Sawan.

Sample name	Location	Lithology	$^{87}Sr/^{86}Sr$	2 SE
JTG†	Saline di Trapani, Sicily	Gypsum	0.709167	0.000011
13112602	Chao Phraya Mueang Rae	Gypsum	0.708110	0.000010
13112603	Chao Phraya Mueang Rae	Gypsum	0.708157	0.000011
13112603'	Chao Phraya Mueang Rae	Gypsum	0.708150	0.000008
13112604	K-Mining	Gypsum	0.708171	0.000010
GYP13 12-13	SCG Mine (core)	Gypsum	0.708156	0.000008
GYP13 15-16	SCG Mine (core)	Gypsum	0.708156	0.000007
GYP13 22-23	SCG Mine (core)	Gypsum	0.708143	0.000014
GYP13 31-32	SCG Mine (core)	Gypsum	0.708169	0.000009
GYP13 37-38	SCG Mine (core)	Anhydrite	0.708152	0.000009
GYP13 43-44	SCG Mine (core)	Anhydrite	0.708144	0.000008
GYP13 49-50	SCG Mine (core)	Anhydrite	0.708136	0.000008
GYP13 57-58	SCG Mine (core)	Anhydrite	0.708144	0.000009

665

666 † JAMSTEC in-house standard of gypsum rock reference material taken from the Saline
667 di Trapani, Sicily.

668 **FIGURE CAPTIONS**

669 **Fig. 1**. Google Earth images of the study site. (A) Regional map showing the location of
670 the study area. (B) Air photo of northeastern Nakhon Sawan Province showing the
671 locations of the three quarries. (C) Air photo of the K-Mining quarry showing sampling
672 locations. (D) Air photo of the Chao Phraya Mueang Rae quarry showing sampling
673 locations. (E) Air photo of the SCG Mine quarry showing GYP13 drilling site.
674
675 **Fig. 2**. (A) Geotectonic subdivision of Thailand (Ueno & Charoentitirat 2011; Ueno *et*
676 *al*. 2012). (B) Distribution of Carboniferous and Permian sedimentary rocks in central
677 Thailand (DMR 1999; Ueno & Charoentitirat 2011). The location of the study site is
678 indicated.
679
680 **Fig. 3**. Photographs of outcrops. (A) Nodular microcrystalline gypsum rock in the Chao
681 Phraya Mueang Rae quarry (location is given in Fig. 1 D) showing sample locations for
682 13112601, 13112602, 13112603 and 13112603', and showing an andesitic dike
683 (horizontal band in the middle of the image) and strong deformation of vertical nodules
684 (lower part of the image). (B) Andesitic dike (13112605) that intruded massive
685 microcrystalline gypsum rock in the K-Mining quarry (location is given in Fig. 1 C).
686 Scale bars are 1 m.
687
688 **Fig. 4**. (A) Lithologic column of well GYP13 at SCG Mine. Drill site is given in Fig. 1
689 E. (B) Split surfaces of the drilled core samples of GYP13. Sampling position of each
690 piece is shown in (A).
691

692 **Fig. 5**. Plane polarized photomicrographs of gypsum and andesitic intrusions. (A)
693 Gypsum crystals and a folded and sheared silicate lamina in a slightly thick section of
694 sample 13112601. (B) A contact between an andesitic dike and microcrystalline gypsum
695 in sample 13112602. (C) Gypsum crystals in a slightly thick section of sample
696 13112603. (D) Andesitic dike in sample 13112605. Gy, gypsum; And, andesitic
697 material; Cal, calcite vein; Chl, chlorite; Dac, dacitic material; Hbl, hornblende
698 (chloritized); Pl, plagioclase (saussuritized); Qz, quartz.
699
700 **Fig. 6**. Element maps showing the contact between sulfate minerals and an andesitic
701 dike (sample 13112602). The distributions of elements are shown as intensities of
702 characteristic X-rays for each element. Each scale bar is 3 mm.
703
704 **Fig. 7**. Secular variations of strontium ($^{87}Sr/^{86}Sr$, middle panel) and sulfate sulfur ($\delta^{34}S$,
705 bottom panel) isotopic compositions in ocean water from 400 to 200 Ma. The $^{87}Sr/^{86}Sr$
706 values (green curve) are from LOWESS (data compiled by McArthur *et al.* 2012), and
707 the $\delta^{34}S$ values of carbonate-associated sulfates (blue curve) and sulfate evaporites (red)
708 were compiled by Kampschulte & Strauss (2004). Horizontal lines indicate the data
709 range for the Nakhon Sawan gypsum samples. The inset in each panel shows secular
710 variations in isotopic compositions during the last 500 Ma (data sources are the same as
711 given above).
712

713 **SUPPORTING INFORMATION**

714 Additional Supporting Information may be found in the online version of this article at

715 the publisher's web-site:

716

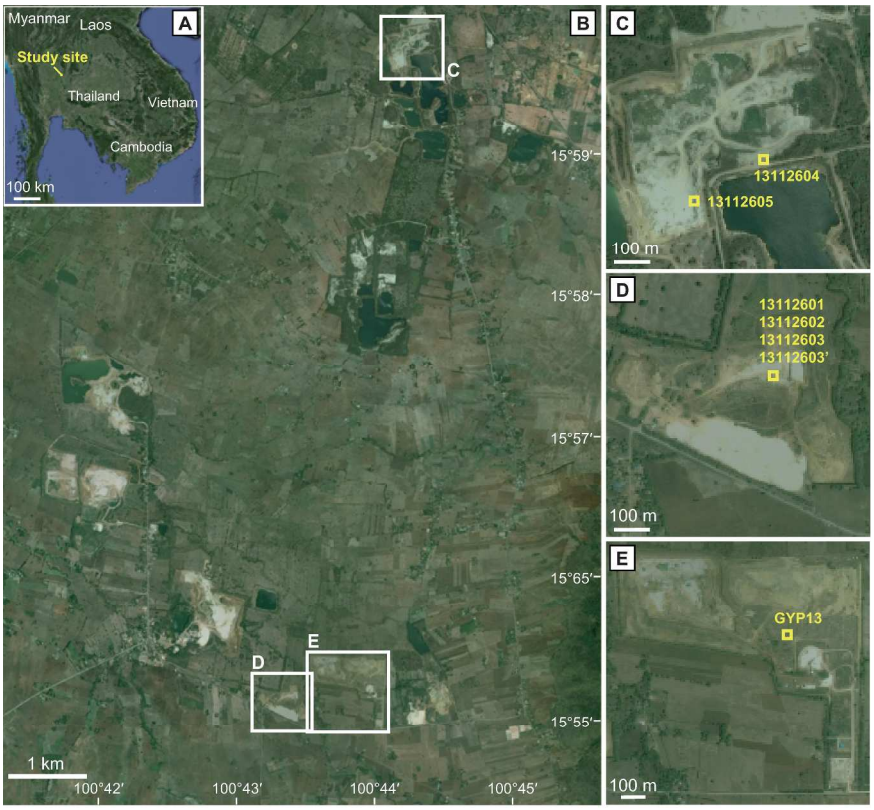

Kuroda et al. Fig. 1

Fig. 1. Google Earth images of the study site. (A) Regional map showing the location of the study area. (B) Air photo of northeastern Nakhon Sawan Province showing the locations of the three quarries. (C) Air photo of the K-Mining quarry showing sampling locations. (D) Air photo of the Chao Phraya Mueang Rae quarry showing sampling locations. (E) Air photo of the SCG Mine quarry showing GYP13 drilling site.
Fig. 1
284x393mm (300 x 300 DPI)

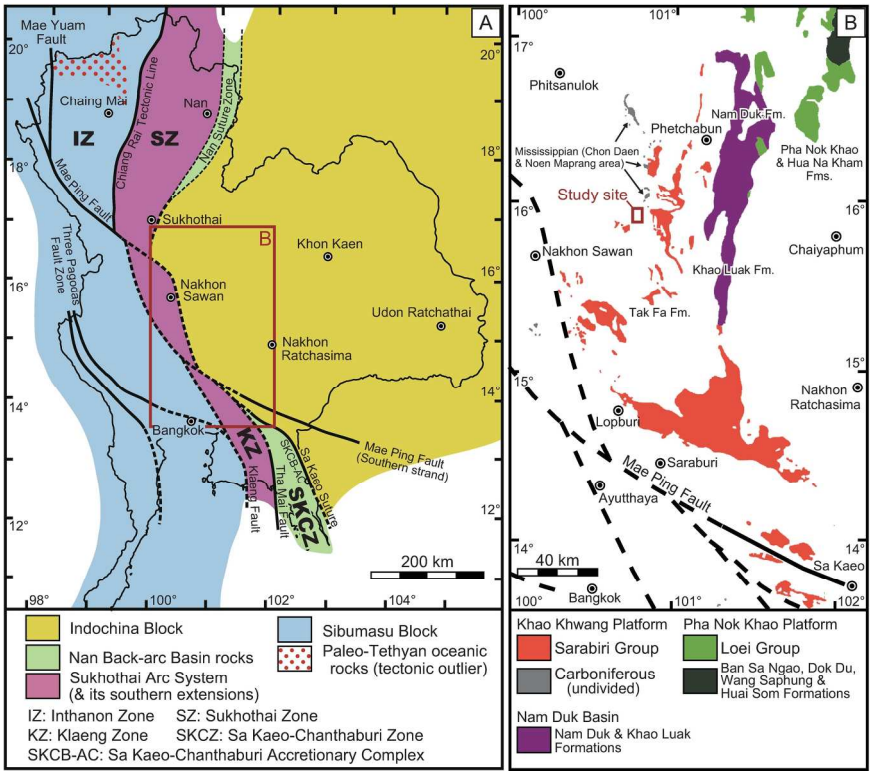

Kuroda et al. Fig. 2

Fig. 2. (A) Geotectonic subdivision of Thailand (Ueno & Charoentitirat 2011; Ueno et al. 2012). (B) Distribution of Carboniferous and Permian sedimentary rocks in central Thailand (DMR 1999; Ueno & Charoentitirat 2011). The location of the study site is indicated.
Fig. 2
201x154mm (300 x 300 DPI)

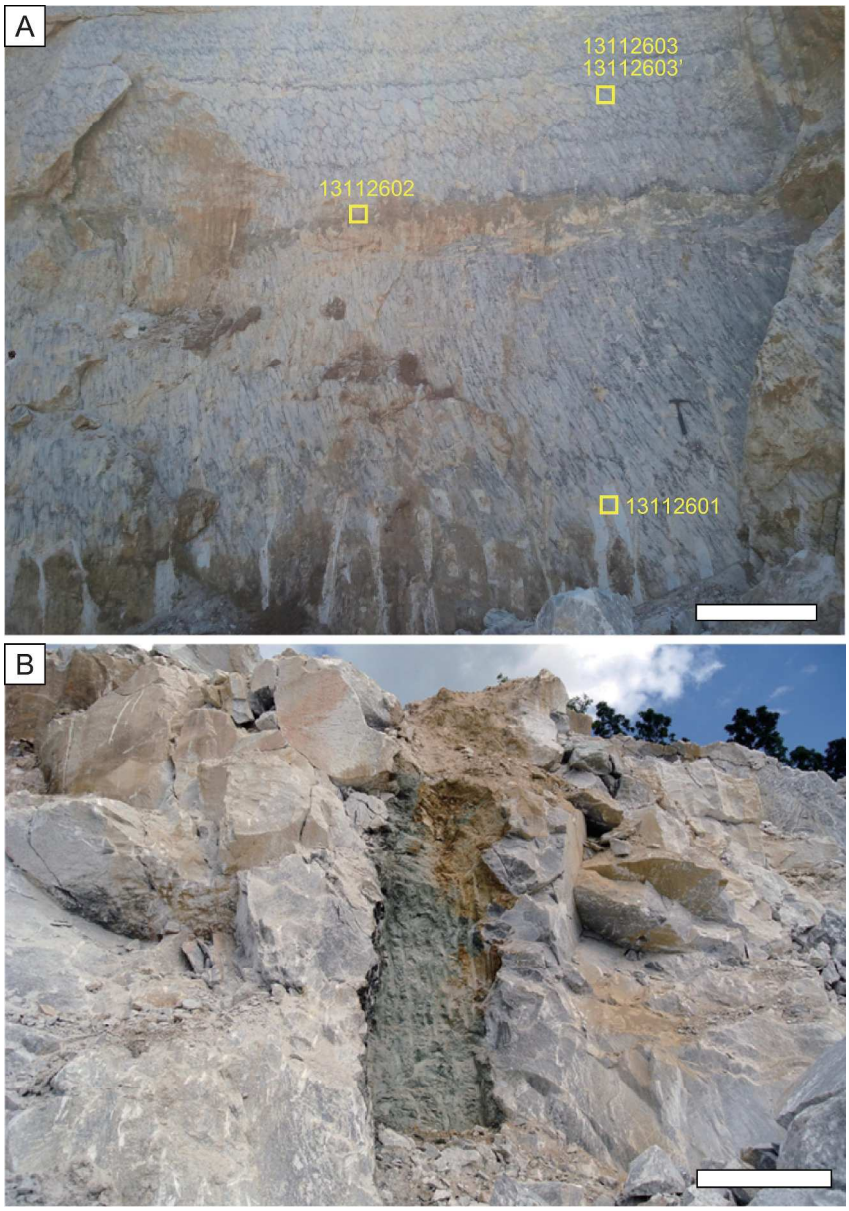

Fig. 3. Photographs of outcrops. (A) Nodular microcrystalline gypsum rock in the Chao Phraya Mueang Rae quarry (location is given in Fig. 1 D) showing sample locations for 13112601, 13112602, 13112603 and 13112603', and showing an andesitic dike (horizontal band in the middle of the image) and strong deformation of vertical nodules (lower part of the image). (B) Andesitic dike (13112605) that intruded massive microcrystalline gypsum rock in the K-Mining quarry (location is given in Fig. 1 C). Scale bars are 1 m.
Fig. 3
292x417mm (300 x 300 DPI)

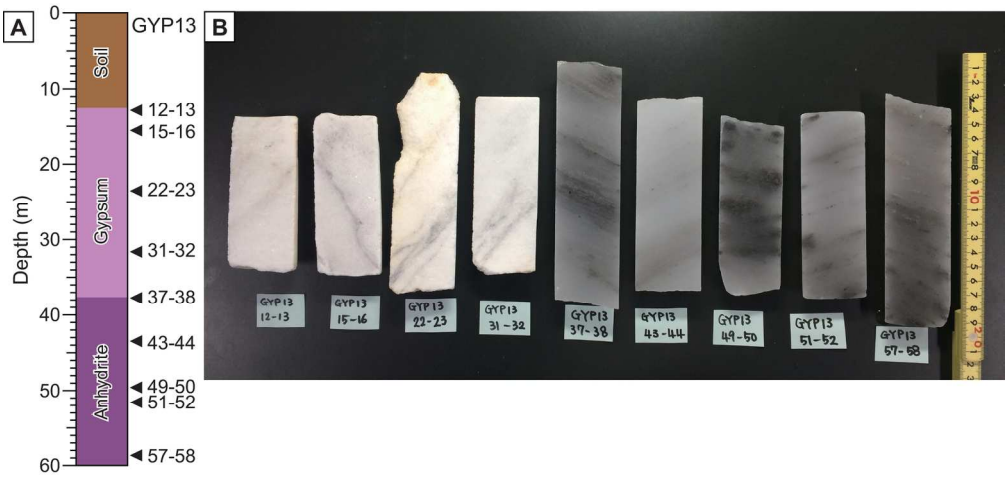

Fig. 4. (A) Lithologic column of well GYP13 at SCG Mine. Drill site is given in Fig. 1 E. (B) Split surfaces of the drilled core samples of GYP13. Sampling position of each piece is shown in (A).
Fig. 4
167x100mm (300 x 300 DPI)

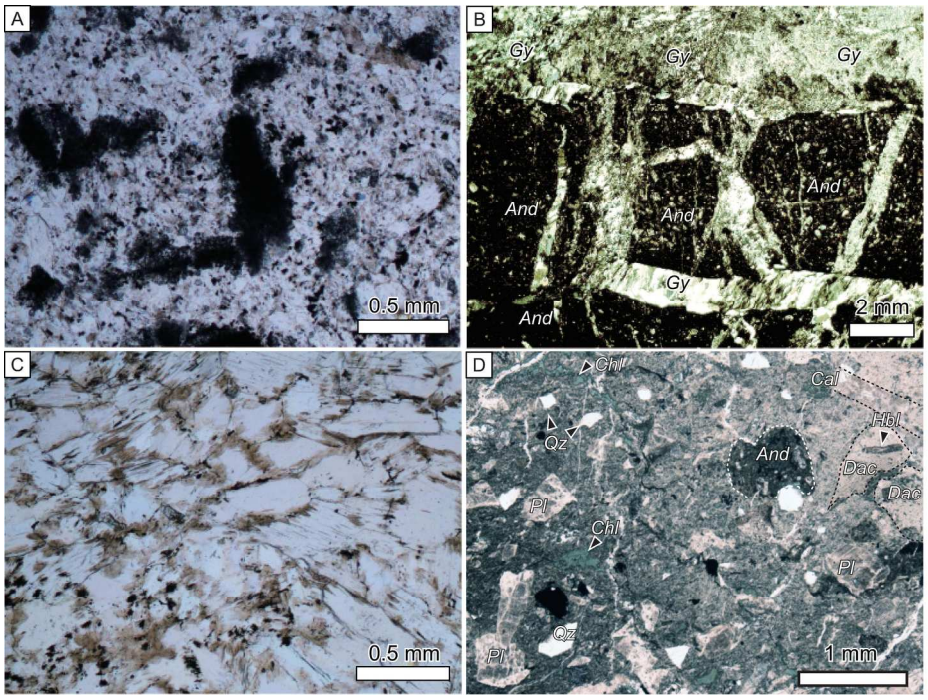

Kuroda et al. Fig. 5

Fig. 5. Plane polarized photomicrographs of gypsum and andesitic intrusions. (A) Gypsum crystals and a folded and sheared silicate lamina in a slightly thick section of sample 13112601. (B) A contact between an andesitic dike and microcrystalline gypsum in sample 13112602. (C) Gypsum crystals in a slightly thick section of sample 13112603. (D) Andesitic dike in sample 13112605. Gy, gypsum; And, andesitic material; Cal, calcite vein; Chl, chlorite; Dac, dacitic material; Hbl, hornblende (chloritized); Pl, plagioclase (saussuritized); Qz, quartz.

Fig. 5
196x135mm (300 x 300 DPI)

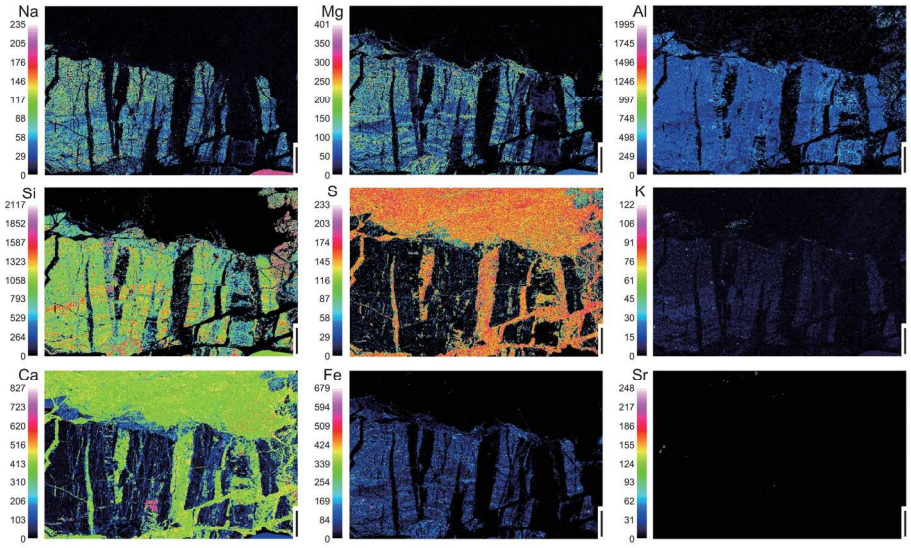

Fig. 6. Element maps showing the contact between sulfate minerals and an andesitic dike (sample 13112602). The distributions of elements are shown as intensities of characteristic X-rays for each element. Each scale bar is 3 mm.
Fig. 6
173x114mm (300 x 300 DPI)

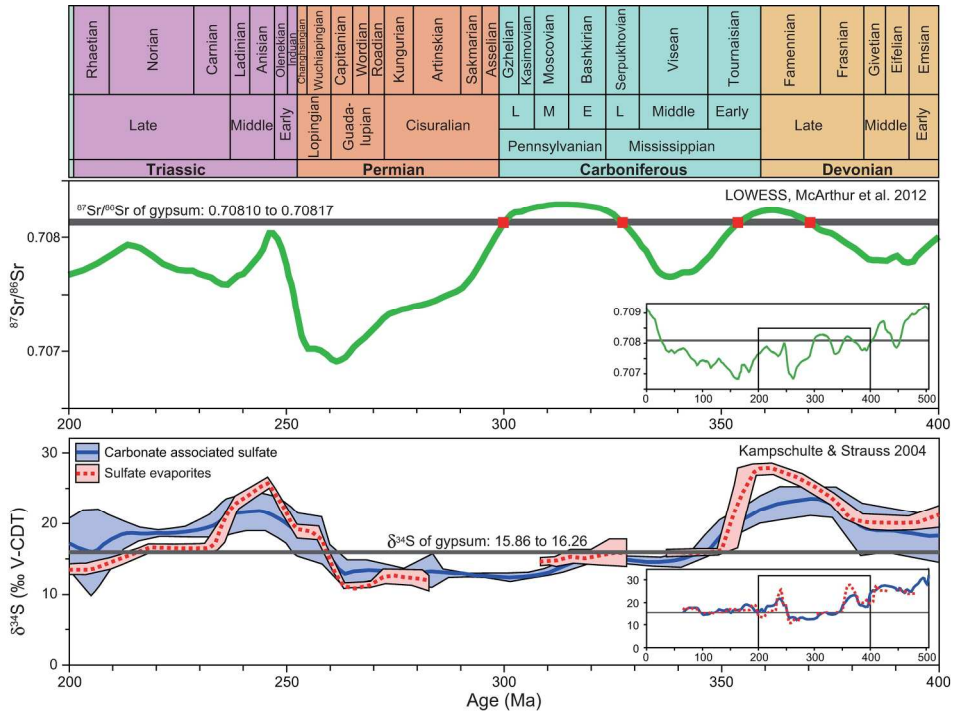

Kuroda et al. Fig. 7

Fig. 7. Secular variations of strontium ($^{87}Sr/^{86}Sr$, middle panel) and sulfate sulfur ($\delta^{34}S$, bottom panel) isotopic compositions in ocean water from 400 to 200 Ma. The $^{87}Sr/^{86}Sr$ values (green curve) are from LOWESS (data compiled by McArthur et al. 2012), and the $\delta^{34}S$ values of carbonate-associated sulfates (blue curve) and sulfate evaporites (red) were compiled by Kampschulte & Strauss (2004). Horizontal lines indicate the data range for the Nakhon Sawan gypsum samples. The inset in each panel shows secular variations in isotopic compositions during the last 500 Ma (data sources are the same as given above).

Fig. 7
205x145mm (300 x 300 DPI)

SUPPORTING INFORMATION

Table S1. Major and trace element compositions of the andesitic dike. Geochemical analyses of the dike were performed by X-ray fluorescence (XRF; Rigaku RIX3000) analysis of fused glass beads at Niigata University.

Major element	SiO_2	TiO_2	Al_2O_3	$Fe_2O_3^*$	MnO	MgO	CaO	Na_2O	K_2O	P_2O_5	Total	L.O.I.
(wt. %)	59.91	0.49	15.26	5.39	0.12	2.33	7.02	1.37	0.51	0.07	100.29	7.2
Trace element	Cr	Nb	Ni	Rb	Sr	V	Y	Zr	Pb	Th		
($\mu g\ g^{-1}$)	107.2	12.3	3.89	3.2	11.65	537.95	102.7	35.305	105.42	13.056	4.399	

L.O.I.: Weight loss on ignition, $Fe_2O_3^*$ is total iron as Fe_2O_3.

Table S2. U–Pb isotopic data (concordia data) for zircon crystals from the andesitic dike (sample 112605). Analyses were performed using LA–ICP–MS.

Grain Number	Th/U	$^{206}Pb/^{238}U$	Error 2σ	$^{207}Pb/^{235}U$	Error 2σ	^{238}U-^{206}Pb age (Ma)	Error 2σ	^{235}U-^{207}Pb age (Ma)	Error 2σ
01	0.70	0.0520 ± 0.0016		0.385 ± 0.036		327.1 ± 10.2		330.6 ± 30.6	
02	0.91	0.0471 ± 0.0013		0.354 ± 0.022		296.7 ± 8.1		307.8 ± 19.2	
04	0.90	0.0583 ± 0.0016		0.471 ± 0.026		365.1 ± 9.8		392.1 ± 21.6	
05	0.87	0.0676 ± 0.0019		0.489 ± 0.032		421.5 ± 11.7		404.3 ± 26.8	
06	0.55	0.0520 ± 0.0014		0.373 ± 0.022		326.7 ± 8.8		322.0 ± 19.0	
07	1.03	0.0686 ± 0.0019		0.533 ± 0.033		427.7 ± 11.9		433.6 ± 27.2	
08	0.48	0.0701 ± 0.0019		0.494 ± 0.029		436.7 ± 11.8		407.9 ± 23.7	
10	0.79	0.0541 ± 0.0018		0.406 ± 0.046		339.6 ± 11.6		346.3 ± 39.4	
11	0.40	0.0656 ± 0.0018		0.516 ± 0.029		409.8 ± 11.3		422.4 ± 24.0	
12	0.44	0.4521 ± 0.0120		9.846 ± 0.382		2,404.7 ± 63.9		2,420.3 ± 93.9	
13	0.89	0.0505 ± 0.0015		0.362 ± 0.031		317.8 ± 9.7		313.6 ± 27.0	
14	0.61	0.0445 ± 0.0016		0.343 ± 0.042		280.7 ± 9.9		299.4 ± 36.4	
16	0.68	0.0453 ± 0.0014		0.340 ± 0.032		285.7 ± 9.0		297.5 ± 28.1	
17	0.30	0.0562 ± 0.0015		0.417 ± 0.025		352.6 ± 9.7		354.2 ± 21.5	
18	0.66	0.0557 ± 0.0016		0.411 ± 0.032		349.2 ± 10.3		349.7 ± 27.0	
19	0.79	0.0493 ± 0.0013		0.366 ± 0.021		310.4 ± 8.4		316.3 ± 18.1	
20	0.57	0.0479 ± 0.0015		0.321 ± 0.030		301.6 ± 9.4		282.9 ± 26.3	
21	0.61	0.0615 ± 0.0018		0.448 ± 0.037		384.5 ± 11.6		375.8 ± 31.1	
22	1.18	0.0387 ± 0.0010		0.296 ± 0.016		244.9 ± 6.5		263.2 ± 14.0	
23	0.77	0.0472 ± 0.0014		0.364 ± 0.028		297.2 ± 8.8		315.4 ± 24.5	
25	0.66	0.0470 ± 0.0014		0.346 ± 0.032		296.3 ± 8.8		301.7 ± 27.6	
26	0.89	0.0366 ± 0.0009		0.267 ± 0.014		231.7 ± 5.8		239.9 ± 13.0	
32	0.35	0.0572 ± 0.0015		0.443 ± 0.026		358.9 ± 9.1		372.3 ± 21.8	
34	0.68	0.0449 ± 0.0018		0.379 ± 0.043		283.1 ± 11.2		326.2 ± 37.2	
35	0.72	0.0458 ± 0.0016		0.354 ± 0.030		288.7 ± 10.2		307.9 ± 26.0	
36	0.67	0.0459 ± 0.0016		0.354 ± 0.030		289.1 ± 10.2		307.4 ± 25.9	
38	0.67	0.0453 ± 0.0018		0.355 ± 0.042		285.8 ± 11.3		308.1 ± 36.3	
40	1.01	0.0533 ± 0.0019		0.410 ± 0.034		334.5 ± 11.8		349.0 ± 29.1	
41	0.82	0.0534 ± 0.0030		0.409 ± 0.043		335.3 ± 19.1		347.8 ± 36.3	
42	0.38	0.0648 ± 0.0036		0.496 ± 0.043		404.8 ± 22.5		409.1 ± 35.1	
43	0.46	0.0602 ± 0.0033		0.471 ± 0.036		377.0 ± 20.7		391.6 ± 30.3	
46	0.11	0.0561 ± 0.0033		0.461 ± 0.061		352.0 ± 21.0		385.3 ± 51.3	
47	0.47	0.0434 ± 0.0028		0.378 ± 0.069		274.1 ± 17.7		325.7 ± 59.5	

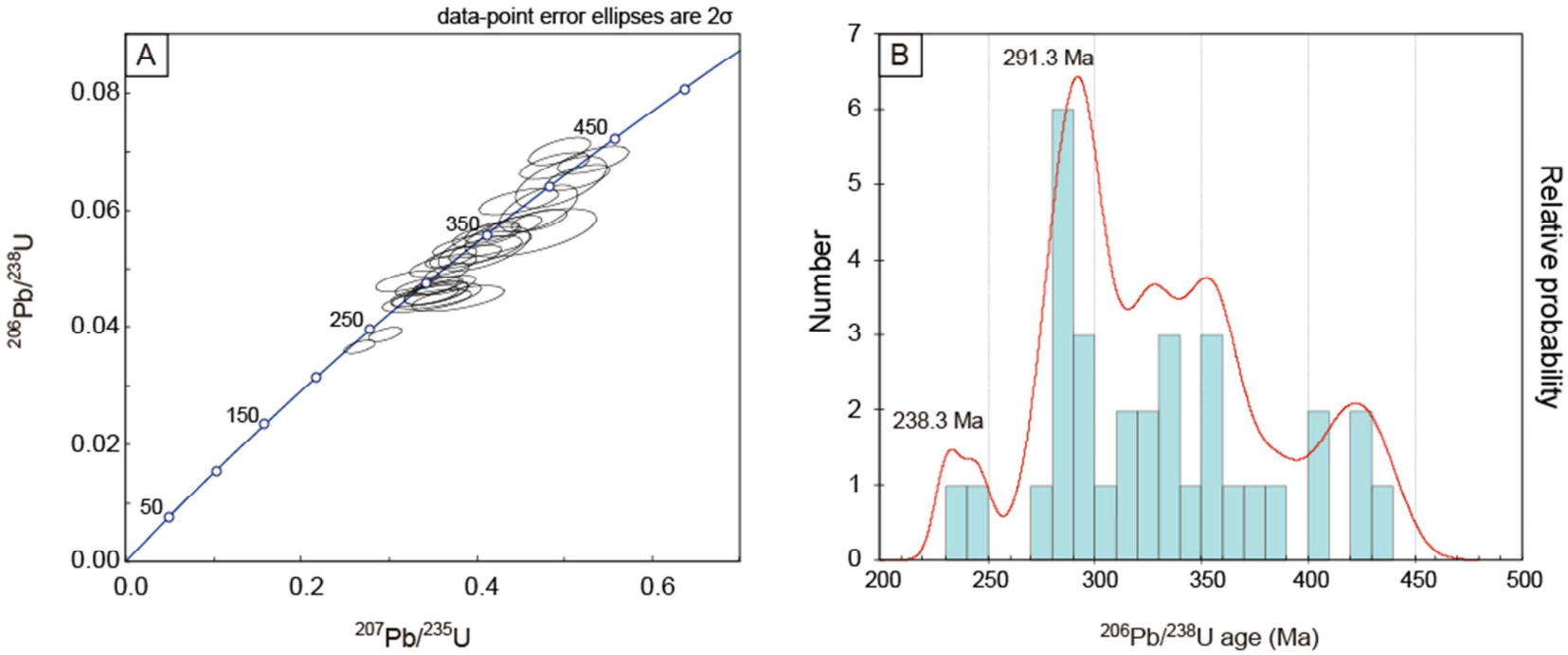

Fig. S1. Analytical data for zircons younger than 500 Ma from the andesitic dike sample 13112605. (A) Concordia diagram. (B) Relative probability plot and age distribution histogram. Analytical errors are present at 2σ.

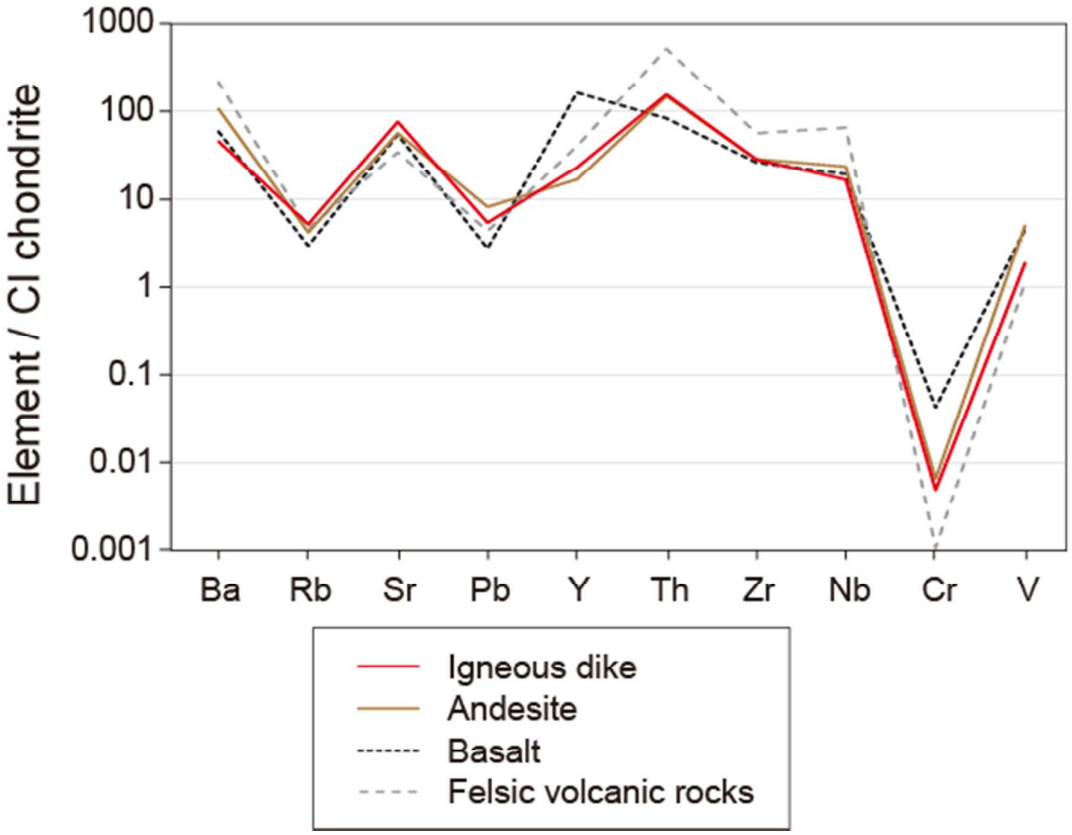

Fig. S2. Trace element composition of the andesitic dike normalized against CI chondrite (Anders and Grevesse 1989). Geochemical data for volcanic rocks in the Sukhothai Arc are from Srichan *et al*. (2009).

REFERENCES

ANDERS E. & GREVESSE N. 1989. Abundance of the elements: Meteoritic and solar. *Geochimica et Cosmochimica Acta* **53**, 197–214.

SRICHAN W., CRAWFORD A.J. & BERRY R.F. 2009. Geochemistry and geochronology of Late Triassic volcanic rocks in the Chiang Khong region, northern Thailand. *Island Arc* **18**, 32–51.